Article

Molecular Cell

Acute Activation of Oxidative Pentose Phosphate Pathway as First-Line Response to Oxidative Stress in Human Skin Cells

Graphical Abstract

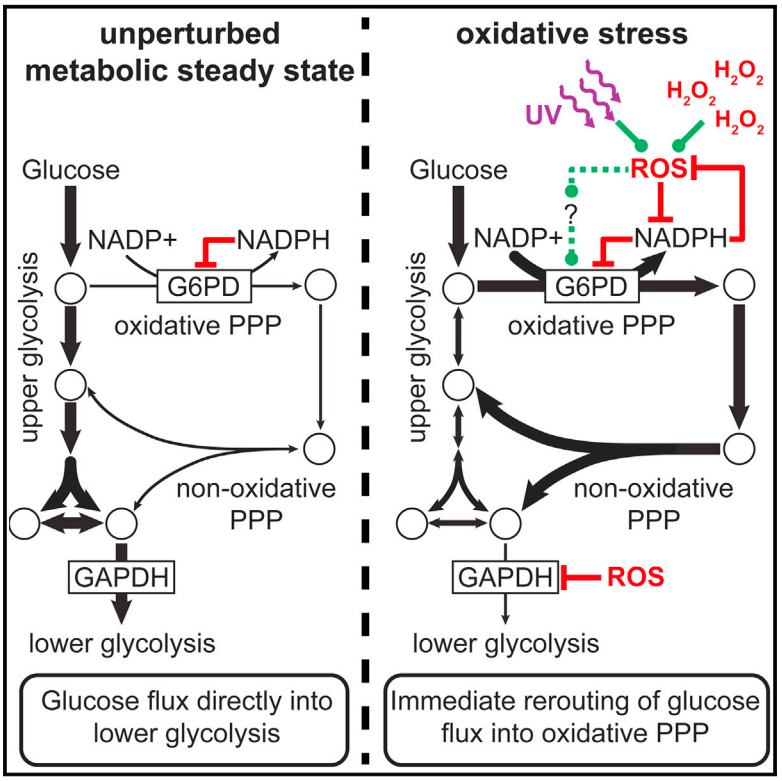

Highlights

- Oxidants induce rerouting of glucose flux into oxidative PPP within seconds
- Initial rerouting is independent of GADPH or PKM2 inhibition
- Multiple cycling of carbon molecules in PPP potentially amplifies NADPH production
- PPP activation might be involved in resistance against ROS-based cancer therapies

Authors

Andreas Kuehne, Hila Emmert, Joern Soehle, ..., Ralph Lucius, Janosch Hildebrand, Nicola Zamboni

Correspondence

Janosch.Hildebrand@Beiersdorf.com (J.H.), zamboni@imsb.biol.ethz.ch (N.Z.)

In Brief

The human skin is continuously exposed to oxidative stress induced by UV irradiation. Kuehne and Emmert et al. report how skin cells reroute glucose flux into the oxidative pentose phosphate pathway as a first-line defense to increase NADPH production, which is essential to prevent oxidative damage.

Kuehne et al., 2015, Molecular Cell *59*, 359–371
August 6, 2015
http://dx.doi.org/10.1016/j.molcel.2015.06.017

CellPress

Molecular Cell
Article

Acute Activation of Oxidative Pentose Phosphate Pathway as First-Line Response to Oxidative Stress in Human Skin Cells

Andreas Kuehne,[1,2,5] Hila Emmert,[3,5] Joern Soehle,[3] Marc Winnefeld,[3] Frank Fischer,[3] Horst Wenck,[3] Stefan Gallinat,[3] Lara Terstegen,[3] Ralph Lucius,[4] Janosch Hildebrand,[3,*] and Nicola Zamboni[1,*]
[1]Institute of Molecular Systems Biology, ETH Zurich, Auguste-Piccard-Hof 1, 8093 Zurich, Switzerland
[2]PhD Program Systems Biology, Life Science Zurich Graduate School, 8093 Zurich, Switzerland
[3]Beiersdorf AG, R&D, Skin Research Center, Unnastrasse 48, Hamburg, 20253 Germany
[4]Christian Albrecht University Kiel, Department of Anatomy, Otto-Hahn-Platz 8, 24118 Kiel, Germany
[5]Co-first author
*Correspondence: Janosch.Hildebrand@Beiersdorf.com (J.H.), zamboni@imsb.biol.ethz.ch (N.Z.)
http://dx.doi.org/10.1016/j.molcel.2015.06.017

SUMMARY

Integrity of human skin is endangered by exposure to UV irradiation and chemical stressors, which can provoke a toxic production of reactive oxygen species (ROS) and oxidative damage. Since oxidation of proteins and metabolites occurs virtually instantaneously, immediate cellular countermeasures are pivotal to mitigate the negative implications of acute oxidative stress. We investigated the short-term metabolic response in human skin fibroblasts and keratinocytes to H_2O_2 and UV exposure. In time-resolved metabolomics experiments, we observed that within seconds after stress induction, glucose catabolism is routed to the oxidative pentose phosphate pathway (PPP) and nucleotide synthesis independent of previously postulated blocks in glycolysis (i.e., of GAPDH or PKM2). Through ultra-short ^{13}C labeling experiments, we provide evidence for multiple cycling of carbon backbones in the oxidative PPP, potentially maximizing NADPH reduction. The identified metabolic rerouting in oxidative and non-oxidative PPP has important physiological roles in stabilization of the redox balance and ROS clearance.

INTRODUCTION

The human skin is exposed to many environmental cues, including UV irradiation and chemical agents, which cause the excessive formation of reactive oxygen species (ROS). These oxidative stress conditions can lead to molecular modifications like lipid peroxidation, protein oxidation, and DNA damage (Kohen and Nyska, 2002), inducing several physiological dysfunctions, ranging from sunburn over skin aging to skin cancer (Finkel, 2003; Finkel and Holbrook, 2000; Kanavy and Gerstenblith, 2011). To fight oxidative stress, cells have developed various anti-oxidative mechanisms. Long-term anti-oxidative responses are a central part of the cellular stress defense and include activation of signaling pathways that dependent on the strength of and damage induced by the stress to initialize either pro-survival gene expression programs for continuous ROS detoxification (e.g., Nrf2) and DNA damage repair (e.g., ATM and p53) or cell-death-inducing programs like apoptosis or necrosis (e.g., NF-κB and p53) (Martindale and Holbrook, 2002; Ray et al., 2012).

Short-term responses are instrumental to alleviate the acute cellular damages induced by oxidative stress, to provide reducing equivalents, and to stabilize cellular redox potentials. This response is actuated by anti-oxidative cellular systems comprising enzymes (e.g., superoxide dismutase, catalase, and glutathione-peroxidase), as well as non-enzymatic antioxidants such as vitamins and reduced glutathione (GSH) (Chen et al., 2012; Finkel and Holbrook, 2000; Kohen and Nyska, 2002). GSH is one of the most important antioxidants and scavenges ROS directly or as co-factor of the glutathione and thioredoxin systems and thereby gets oxidized to glutathione disulfide (GSSG) (Fang et al., 2002; Stincone et al., 2014). Reduced nicotinamide adenine dinucleotide phosphate (NADPH)—which is produced in different biochemical pathways, including the pentose phosphate pathway (PPP), the citric acid cycle (TCA cycle), and folate metabolism (Fan et al., 2014; Ying, 2008)—is involved in continuously replenishing the GSH pools as co-factor of glutathione reductase (Pai and Schulz, 1983; Rescigno and Perham, 1994) and additionally in keeping catalase in its active form (Hillar and Nicholls, 1992; Kirkman et al., 1987). Glucose-6-phosphate dehydrogenase (G6PD) and 6-phosphogluconolactonase (6PGDH) in the oxidative branch of the PPP (oxidative PPP) are the major sources of NADPH in most tissues and are therefore essential for maintaining redox homeostasis (Stincone et al., 2014). Recent studies demonstrated that a short-term anti-oxidant response can be mediated by redox-sensitive enzymes in lower glycolysis (e.g., by pyruvate kinase M2 [PKM2] in cancer cells or by glyceraldehyde 3-phosphate dehydrogenase [GAPDH] in baker's yeast and mammalian cells (Anastasiou et al., 2011; Colussi et al., 2000; Ralser et al., 2007, 2009). In both cases, oxidation of a cysteine residue caps the glycolytic flux and enables swift accumulation of intermediates in the

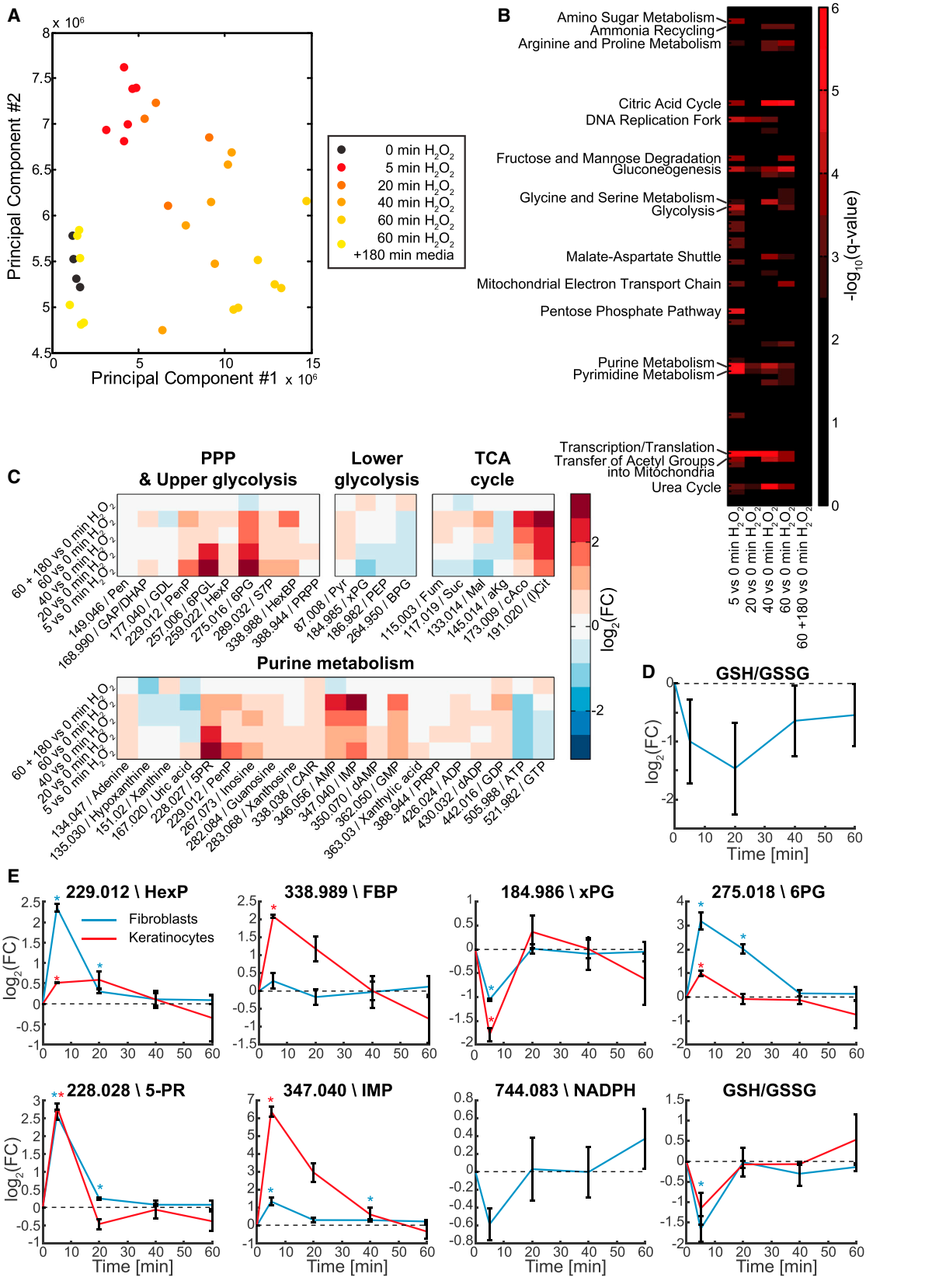

(legend on next page)

PPP and likely promotes nucleotide synthesis for DNA damage repair.

We set out to characterize the short-term metabolic response of human skin fibroblasts and keratinocytes (i.e., the main cellular constituents of human skin) to oxidative stress induced by H_2O_2 and UV irradiation. Combining time-resolved metabolomics, ultra-short ^{13}C labeling experiments, and expression measurements, we found that upon oxidative stress, metabolic flux is immediately rerouted from glycolysis into oxidative PPP and purine metabolism by activation of G6PD independently of a block in lower glycolysis or transcriptional regulation. This activation maximizes the flux of sugar phosphates in the oxidative PPP, potentially through multiple cycling, and thus immediate production of NADPH to fulfill acute demand for reducing equivalents.

RESULTS

Fibroblasts React to H_2O_2 Treatment with Immediate Metabolic Changes in Carbohydrate and Purine Metabolism

To gain a comprehensive picture of the metabolic response of human skin cells to oxidative stress, we treated primary human skin fibroblasts and keratinocytes for 0, 5, 20, 40, and 60 min with 500 μM H_2O_2 (Figure S1A). Intracellular metabolites were analyzed by non-targeted metabolite profiling using flow injection time-of-flight mass spectrometry (Figure S1A) (Fuhrer et al., 2011). This method allows monitoring of a large number of metabolites both in central carbon metabolism and peripheral pathways (i.e., amino acid metabolism, nucleotide biosynthesis, or urea cycle) (Figure S1B). In total, 9,997 ions with unique mass-to-charge ratio were detected and annotated to metabolites listed in the human metabolome database (HMDB) version 3.0 (Wishart et al., 2013) using a strict tolerance of 0.001 amu and excluding adducts. Since our method does not allow distinguishing between metabolites with identical molecular weights, 884 ions matched to 2,570 metabolites listed in the HMDB. Consecutive analysis of the data was performed only on the 884 annotated ions (Table S1 and S2).

To qualitatively assess the dynamics and timing of the metabolic response to oxidative stress, we performed a principal-component analysis of the metabolome data (fibroblasts: Figure 1A; keratinocytes: Figure S3B). Changes in metabolism were observed already after 5 min and steadily progressed with exposure to H_2O_2. Most metabolic changes reverted completely after removal of the stress (60 min H_2O_2 + 180 min control media), indicating that the metabolic changes observed after a short treatment are reversible. A pathway enrichment analysis of the metabolites changing at each time point (compared to untreated controls) revealed strong enrichment for specific metabolic pathways, namely glycolysis, gluconeogenesis, TCA cycle, PPP, purine metabolism, and pyrimidine metabolism (Figures 1B and S3D).

The changes in central carbon and nucleotide metabolism exhibited a high degree of similarity in both cell types and had the largest magnitude. A closer look at the metabolites in these pathways revealed that in glycolysis hexose phosphates, hexose bisphosphates, and glyceraldehyde 3-phosphate (GAP)/dihydroxyacetone phosphate (DHAP) were elevated, while concentrations of 2/3-phosphoglycerate (xPG) and phosphoenolpyruvate (PEP), metabolites of the lower glycolysis, decreased (Figures 1C and S3F). The strongest short-time difference was observed for 6-phosphoglucono-D-lactone (6PGL) and 6-phosphogluconate (6PG) in the oxidative branch of the PPP (Figures 1C and S3F). The levels of metabolites of the non-oxidative branch of the PPP (i.e., erythrose 4-phosphate [E4P], sedoheptulose 7-phosphate [S7P], and pentose phosphates) showed a synchronous but attenuated increase. The increase in PPP metabolites was paralleled by a strong accumulation of the purine precursor 5-phosphoribosylamine (5PRA), suggesting an immediately increased purine de novo biosynthesis possibly needed for DNA damage repair. In contrast, the changes in nucleotides were delayed and progressive in time. An overall decrease of nucleoside triphosphates (ATP and GTP) and an increase of nucleoside monophosphates and diphosphates (Tiwari et al., 2002) emphasized the cellular needs during stress defense, including generation of nucleotide precursors for repair of oxidative-stress-induced DNA damage, generation of reducing equivalents for clearance of ROS, and reduction of endogenous ROS production. Notably, NADPH and $NADP^+$ were undetectable in the majority of the experiments, and glutathione exhibited a valley in reduction state after 20 min that seemingly recovered with longer H_2O_2 exposure in fibroblasts (Figure 1D).

Most metabolome changes reverted within 3 hr after exposing cells to H_2O_2 for 60 min (Figures 1C and S3F). When fibroblasts and keratinocytes were treated transiently for only 5 min with

Figure 1. Metabolic Response of Human Skin Cells upon Exposure to Oxidative Stress

Fibroblasts and keratinocytes were treated with 500 μM H_2O_2 for 0, 5, 20, 40, or 60 min or for 60 min followed by a cultivation in H_2O_2-free media for 180 min.

(A) Principal-component analysis of intracellular metabolites in H_2O_2-treated fibroblasts.

(B and C) (B) Metabolic pathway enrichment analysis and (C) metabolic changes in selected pathways comparing H_2O_2-stressed (t = 5–240 min 500 μM H_2O_2) and unstressed cells (t = 0 min H_2O_2).

(A–C) Metabolite data of one representative of three individual experiments.

(D) Glutathione redox state in fibroblasts during H_2O_2 treatment.

(E) Metabolic changes in PPP and purine metabolism in fibroblasts and keratioincytes treated with a 5 min pulse of 500 μM H_2O_2.

(D and E) Plots show mean ± SEM, including results of a paired t test comparing metabolite levels at x versus 0 min treatment (*$p < 0.05$) of three individual experiments with three biological replicates. (Related to Figure S1–S3; Table S1 and S2.) Abbreviations: (l)Cit, (Iso)citrate; 5PR, 5-phosphoribosylamine; 6PG, 6-phosphogluconate; 6PGL, 6-phosphoglucono-D-lactone; aKg, α-ketoglutarate; BPG, biphosphoglycerate; cAco, cis-aconitate; CAIR, 1-(5-Phospho-D-ribosyl)-5-amino-4-imidazolecarboxylate; DHAP, dihydroxyacetone phosphate; E4P, erythrose 4-phosphat; Fum, fumarate; GAP, glyceraldehyde 3-phosphate; GDL, gluconolactone; GSH, reduced glutathione; GSSG, oxidized glutathione; HexBP, hexose bisphosphates; HexP, hexose phosphates (e.g., glucose-6-phosphate, fructose-6-phosphate); IMP, inosine monophosphate; Mal, malate; Pen, pentoses; PenP, pentose phosphates; PEP, phosphoenolpyruvate; PRPP, 5-Phosphoribosyl diphosphate; Pyr, pyruvate; S7P, sedoheptulose 7-phosphate; Suc, succinate; xPG, 2/3-phosphoglycerate.

500 μM H_2O_2 (Figures 1E, S3E, and S3G), the metabolite levels, including NADPH and the GSH:GSSG ratio, reverted to the pre-stress state within 30 min. This suggests that the observed metabolic shift is transient and not transcriptionally regulated. To confirm this hypothesis, we analyzed gene expression of pertinent enzymes after H_2O_2 treatment. Known stress-responsive genes such as p53-dependent cell cycle regulator GADD45 and CDK inhibitor p21 (CDKN1a) (Liebermann and Hoffman, 2008; Qiu et al., 1996; Xiong et al., 1993) showed elevated gene expression 4 hr after H_2O_2 treatment (Figure S2), confirming the stress-induced cell cycle arrest. In contrast, expression of all analyzed enzymes in central carbon metabolism and purine biosynthesis was not significantly altered within 60 min of H_2O_2 treatment, indicating that the observed metabolic adaptations are indeed independent of transcriptional control (Figure S2).

Rerouting of Metabolites from Glycolysis to PPP Occurs before GAPDH Inhibition Leads to an Accumulation of Metabolites in Upper Glycolysis

The metabolite alterations in glycolysis and TCA cycle are compatible with the previously shown oxidative inhibition of GAPDH (Colussi et al., 2000; Ralser et al., 2007, 2009; Shenton and Grant, 2003), which we could confirm with an enzymatic assay (Figures S4A and S4B). We wondered whether this would be sufficient to explain all observed changes in glycolysis and PPP. To accurately resolve the onset of metabolic reconfiguration, we performed two experiments to determine timing and sensitivity of metabolite responses. First, we sampled human fibroblasts and keratinocytes at 1 min intervals for up to 5 min treatment with 500 μM H_2O_2. Metabolites of glycolysis and PPP were extracted and quantified by targeted liquid chromatography-tandem mass spectrometry (LC-MS/MS) (Buescher et al., 2010), and for each metabolite we determined the time $T_{1/2}$ at which half of the maximum fold change is attained. Second, we measured the level of the same metabolites in fibroblasts and keratinocytes exposed for 5 min to H_2O_2 at different concentrations ranging from 0 to 500 μM. The resulting data were analyzed to determine the half maximal effective H_2O_2 concentration (EC_{50}) (Figure 2, S4C, and S4D; Table S5).

The results indicated that 6PG, G6P, glycerol phosphates, PEP, and xPG are the metabolites with the highest sensitivity for fibroblasts and 6PG, ADP, R5P, Ru5P, S7P, xPG, and Xu5P for keratinocytes, with an EC_{50} < 100 μM H_2O_2 and $T_{1/2}$ < 1.5 min. In fibroblasts, intermediates of the non-oxidative PPP had similar $T_{1/2}$ but were clearly less sensitive to H_2O_2 concentrations (EC_{50} > 200 μM H_2O_2). Oxidative inhibition of GAPDH likely causes the quick depletion of xPG and PEP but fails to explain the sharp and H_2O_2-sensitive increase in 6PG. It was suggested that inhibition of glycolytic flux at GAPDH or PKM2 leads to an accumulation of upper glycolytic metabolites inducing an increased flux into PPP (Anastasiou et al., 2011; Ralser et al., 2007, 2009). However, the intermediates upstream of GAPDH (i.e., FBP and F6P) did not increase as quickly and as sensitively ($T_{1/2} \geq$ 1.5 min or n.d., EC_{50} > 250 or n.d. for fibroblasts and $T_{1/2} \geq$ 1 min, EC_{50} > 170 for keratinocytes) and therefore cannot cause a 16-fold increase in 6PG. Instead, our data indicate that the oxidative PPP is directly activated immediately upon oxidative stress.

Knockdowns of G6PD, Transaldolase, and Transketolase Impair Metabolic Response to Oxidative Stress

The regulation of the acute metabolic response in glycolysis and PPP upon exposure to oxidative stress is more complex than thus far described. The apparent activation of oxidative PPP would presume that the net flux in PPP proceeds toward glycolysis. In contrast, inhibition of GAPDH or PKM2 was suggested to lead to an accumulation of upper glycolytic metabolites causing an increased flux from glycolysis into both the oxidative and non-oxidative PPP to promote NADPH generation and nucleotide synthesis (Anastasiou et al., 2011; Ralser et al., 2009). To investigate the detailed rerouting and infer the directionality of fluxes in oxidative and non-oxidative PPP, we analyzed the metabolic response to H_2O_2 in fibroblasts depleted of G6PD, transketolase (TK), and transaldolase (TA) by siRNA-mediated silencing.

In G6PD knockdowns, the increase in 6PGL and 6PG during stress was significantly attenuated, demonstrating that their accumulation is caused by an activation of the oxidative PPP involving G6PD (Figure 3). The increase of pentose phosphates and S7P after H_2O_2 stress in the G6PD knockdown was also reduced, suggesting that the accumulation of metabolites in the PPP is driven through the oxidative branch and not from glycolysis via reversed TK and TA. Accordingly, single and double knockdowns of TK and TA lead to even stronger accumulation of pentose phosphates and 5PRA pools after oxidative stress compared to H_2O_2-treated control cells. Furthermore, metabolites in upper glycolysis increased less pronouncedly after oxidative stress in TA and TK single and double knockdown cells (Figure 3). All these results suggest that under oxidative stress the oxidative PPP is activated, and the accumulation in pentose phosphates and possibly purine biosynthesis results from an increased higher flux from 6PG. A portion of the carbon flux from the oxidative branch returns to glycolysis through TA and TK, leading to delayed accumulation of upper glycolytic metabolites.

Oxidative Stress Induced Immediate Flux Rerouting and Reversal in PPP

We attempted to corroborate our model using ^{13}C-glucose. We initially characterized PPP fluxes in unperturbed human skin fibroblasts with 100% [1-^{13}C]-glucose sampling at several time points after switching to the medium containing the ^{13}C-tracer. Mass isotopomer distributions (MIDs) of glycolytic and PPP metabolites were determined by targeted LC-MS/MS (Buescher et al., 2010; Rühl et al., 2012). Within 10 min of labeling, the ^{13}C enrichment of G6P reached its steady-state value of ~90% (Figure 4A). Biosynthesis of pentose phosphates via oxidative PPP leads to unlabeled molecules ($P5P_{m+0}$), while biosynthesis through the non-oxidative branch (TK and TA) generates the high fraction of $P5P_{m+1}$ and $P5P_{m+2}$ (Figure S5A). The measured steady-state $R5P_{m+1}$ and $R5P_{m+2}$ accounted for 35% ± 7% and 15% ± 1%, respectively (Figure 4A). This proves that in normal conditions P5P are synthesized both through the oxidative and non-oxidative PPP pathways. Next, we wondered whether P5P are also converted to glycolytic intermediates through the non-oxidative branch. In the same data, we observed that triose-phosphates were to 50% labeled once

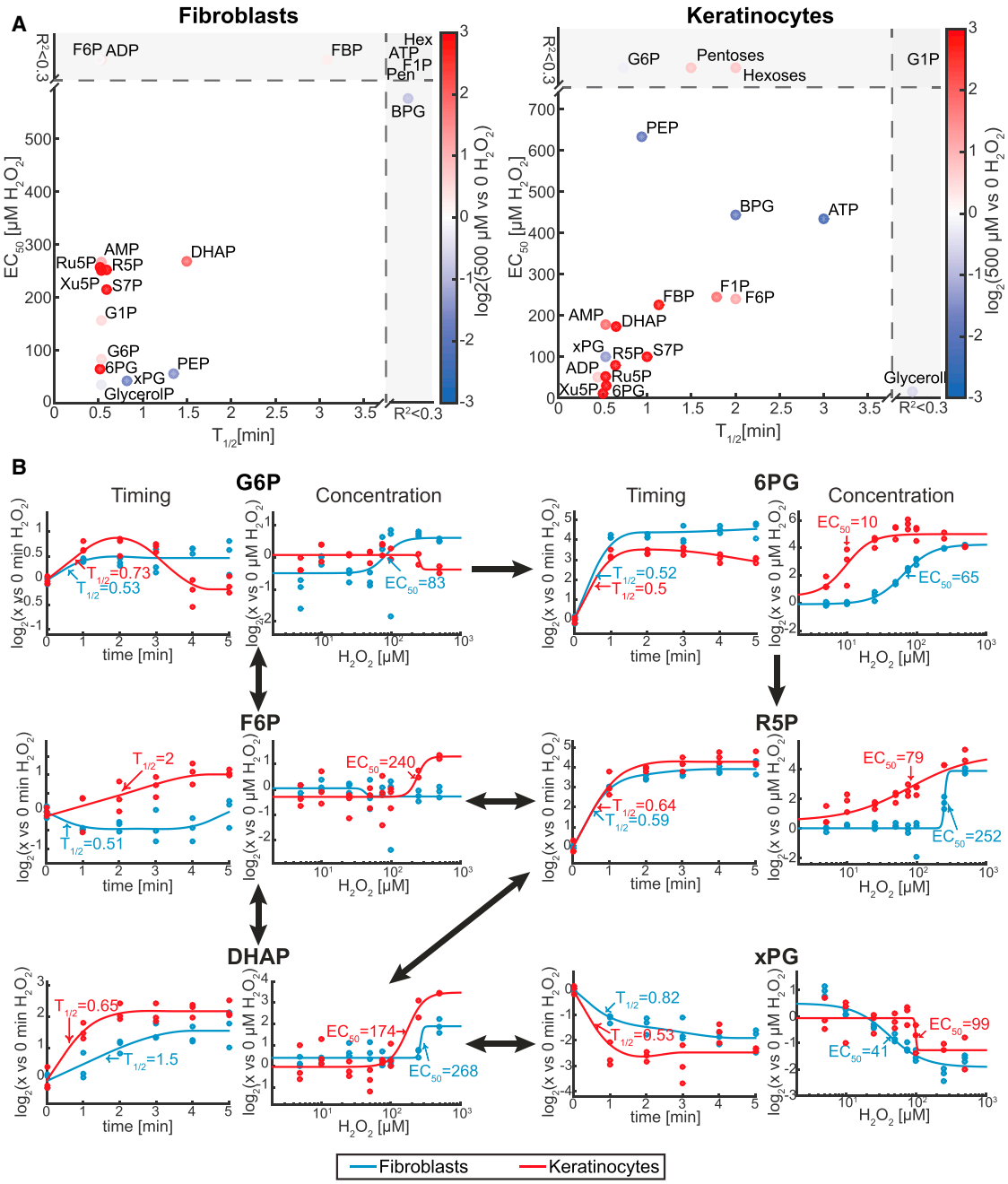

Figure 2. Temporal and Concentration Dependent Sensitivity of Metabolic Changes in PPP and Glycolysis

Fibroblasts and keratinocytes were treated with 500 μM for up to 5 min (temporal analysis) or treated for 5 min with H_2O_2 dilutions ranging from 0 to 500 μM (concentration dependency analysis).

(A) Overview of concentration dependency (EC_{50}) and temporal sensitivity ($T_{1/2}$) determined by fitting of sigmoidal dose-response and quadratics splines to targeted metabolite measurements of selected metabolites of a H_2O_2 dilution series and H_2O_2 short time experiment.

(B) Data (dots) of selected metabolic changes in PPP and upper glycolysis including cubic spline and sigmoidal dose-response fits (lines). (Related to Figure S4; Table S5.) Abbreviations: F1P, fructose-1-phosphate; F6P, fructose-6-phosphate; FBP, fructose-1,6-bisphosphate; G1P, glucose-1-phosphate; G6P, glucose-6-phosphate; R5P, ribose-5-phosphate; Ru5P, ribulose-5-phosphate; Xu5P, xylulose-5-phosphate; Hex, hexoses; Pen, pentoses.

(e.g., PEP_{m+1} in Figure 4A). This reflects the theoretical pattern obtained from cleavage of [1-^{13}C]-glucose in glycolysis (Figure S5A). Accordingly, we estimated that only 4.7% ± 2.7% of triose-phosphates originated through the PPP (Figure 4B). Overall, the [1-^{13}C]-glucose experiments indicate that in unperturbed skin fibroblasts, the synthesis of P5P through both PPP

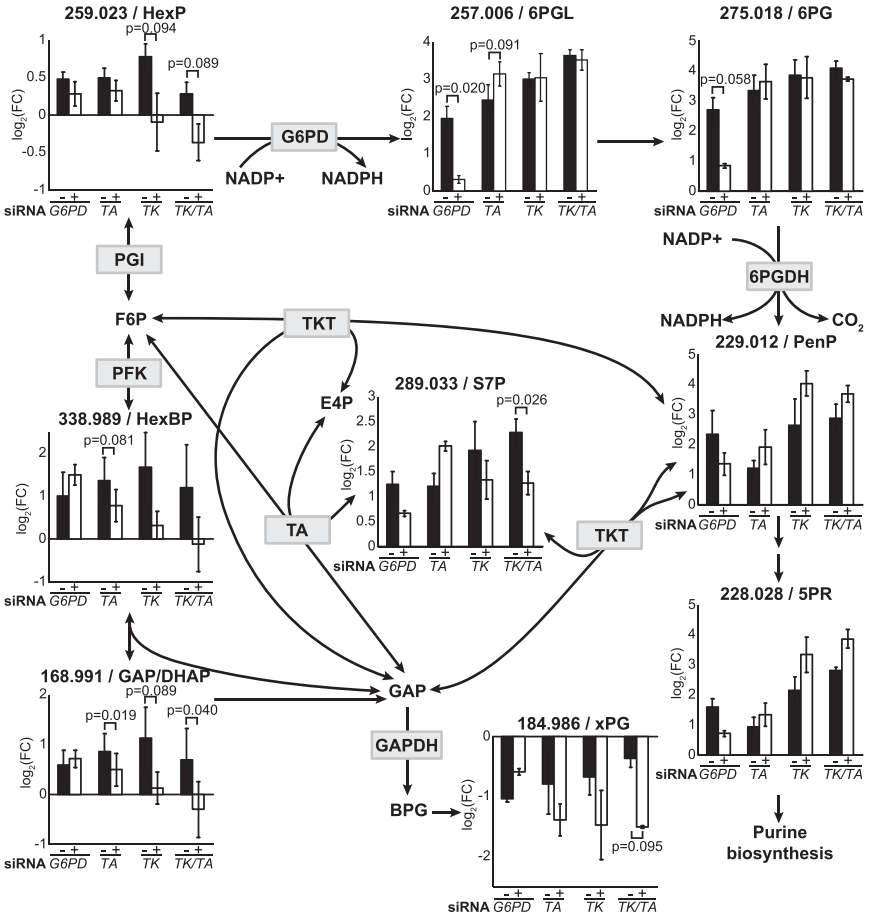

Figure 3. Influence of G6PD-, TK-, TA-, and TK/TA-Knockdown on Metabolic Changes in the PPP and Glycolysis upon Oxidative Stress

Shown are the relative changes of metabolite levels comparing untargeted metabolite measurements after and before exposure to 5 min of 500 μM H_2O_2 in fibroblasts transfected with control siRNA (–) or siRNA targeting (+) either G6PD, TK, TA, or both TK and TA. Plots show mean values ± SEM of the relative metabolite changes, including p values of a paired t test (all $p < 0.1$ are shown) of three individual experiments with each three biological replicates.

branches is balanced to fulfill biosynthetic demand of precursors for, for example, nucleotides and aromatic amino acids.

The extremely transient character of the metabolic response to oxidative stress forced us to rely on non-stationary ^{13}C experiments and sample for up to 10–30 min. This is perhaps still too slow to precisely address the fast dynamics, but it is the time required to have sufficient propagation of ^{13}C in metabolism (Figure 4A). To verify activation of oxidative PPP and overflow of P5P to glycolysis through the non-oxidative PPP branch, we labeled skin fibroblasts with medium containing 50% [U-^{12}C]-glucose and either 50% [1-^{13}C]-glucose or 50% [2-^{13}C]-glucose or medium with 100% [1,2-^{13}C]-glucose and skin keratinocytes with medium containing 50% [U-^{12}C]-glucose and 50% [1,2-^{13}C]-glucose and treated them with or without 500 μM H_2O_2. The measured MIDs were compared to theoretical MIDs calculated for the extreme scenarios with all G6P entering either glycolysis or oxidative PPP (Figures 4C and S5B; Table S6; Supplemental Experimental Procedures).

Upon oxidative stress, the MID of F6P in the [1-^{13}C]-glucose experiment showed an increased $F6P_{m+0}$ fraction coupled to a decreased $F6P_{m+1}$ fraction. In contrast, the MID of F6P in the [2-^{13}C] and [1,2-^{13}C]-glucose experiments showed a slight decrease in $F6P_{m+1}$ and slight increase in $F6P_{m+2}$ (Figures 4C and S5C; Table S6). This change, backed by data for pentose phosphates, S7P, FBP, and DHAP (Figures 4C, S5B, and S5C; Table S6), verified during stress a carbon flux through G6PD transiting the PPP and eventually disemboguing in glycolysis in both fibroblasts and keratinocytes. The kinetics of ^{13}C-propagation to lower glycolysis (BPG, PEP, and xPG; Figure 4C; Table S5) also demonstrated that GAPDH activity is not completely blocked, and glycolysis can proceed.

Upon strong cycling of carbon through oxidative and non-oxidative PPP, a fraction of carbon backbones may be converted back to G6P by the reversible phosphoglucoisomerase (PGI) and cycle again through oxidative PPP to further increase NADPH production. Exploiting the loss of the 1-C of glucose in the oxidative PPP and the measured $6PG_{m+0}$ fraction of the [1-^{13}C] glucose experiment (Figure S5B), we estimated the relative contribution of unlabeled hexose phosphates ($f_{cycling}$) to the oxidative PPP to increase from 10.6% ± 5.9% in unperturbed cells to 32.2% ± 12.6% in the initial 10 min with 500 μM H_2O_2 (Figure 4D). We wanted to confirm this increased cycling of carbon backbones using the [1,2-^{13}C]-glucose labeling data. While for keratinocytes we observe a similar increase from 11.1% ± 1.1% in unperturbed cells to 44.2% ± 4.6% in the initial 10 min with 500 μM H_2O_2, cycling flux in fibroblasts did not change (from 29.6% ± 2.0% in unperturbed cells to 27.8% ± 0.3%) (Figure S5D). Notably, the apparently high cycling of almost 30% in unperturbed fibroblasts is caused by high background noise in the m+0 and m+1 measurement, which is close to detection limit. This problem doesn't occur in perturbed cells because of the much higher 6PG levels upon stress. Therefore, to exclude that unlabeled 6PG in the [1-^{13}C]-glucose experiments originates from mobilization of storage carbon or other unlabeled sources to G6P, we performed a control experiment with [1-^{13}C]-glucose and fibroblasts with double TK/TA knockdown. In contrast to wild-type fibroblasts, cells harboring TK/TA double knockdowns had no increased $6PG_{m+0}$ after induction of oxidative stress, demonstrating that the increase in $6PG_{m+0}$ in wild-type fibroblasts indeed originates from multiple cycling of carbon backbones in the PPP (Figures 4E, S5E, and S5F). With this mechanism, NADPH availability can be increased transiently to fulfill an acute demand.

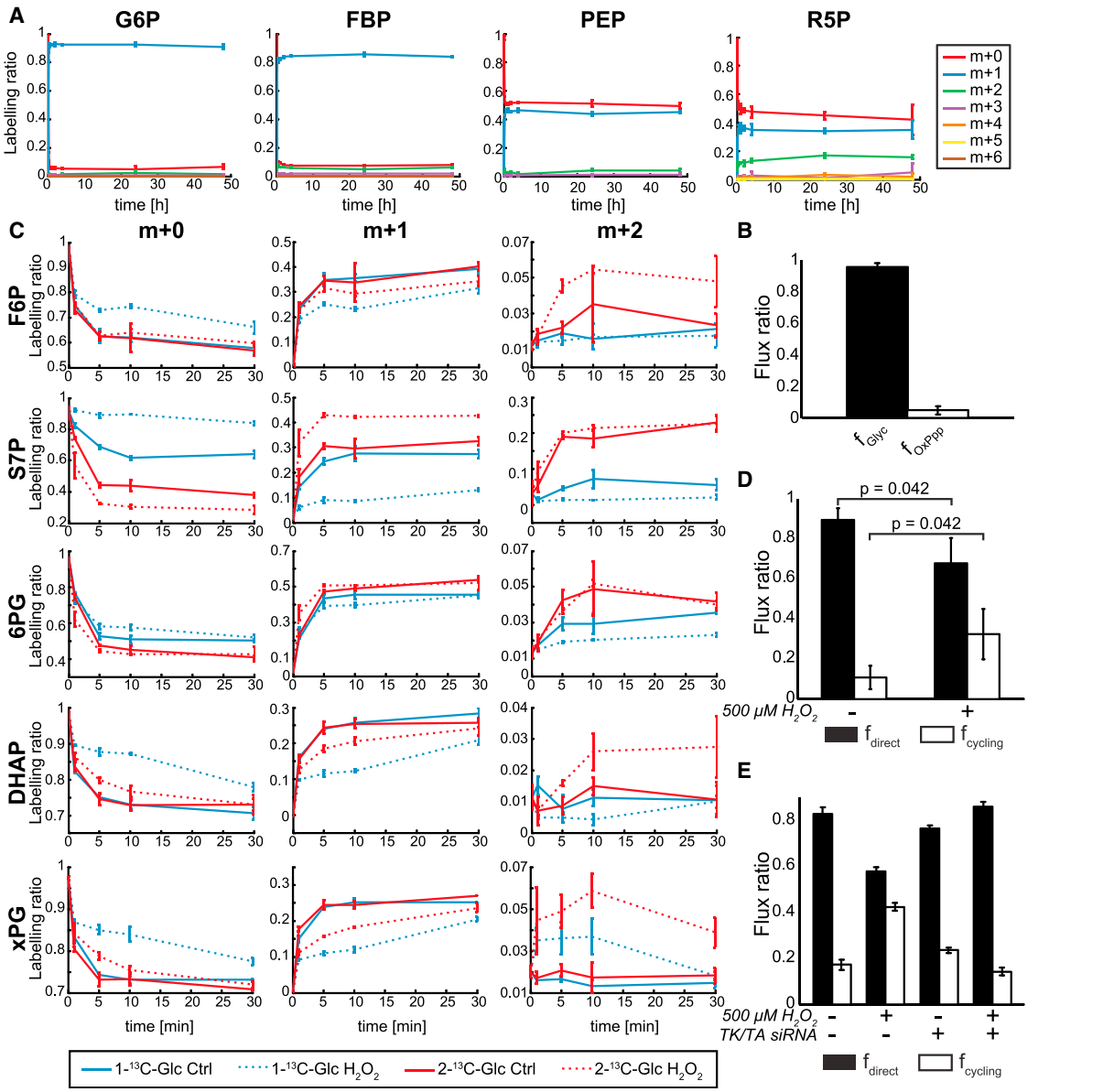

Figure 4. Analysis of Glycolytic and Oxidative PPP Flux in the Unperturbed Metabolic Steady State and after Exposure to Oxidative Stress in Human Skin Fibroblasts

(A) MID of glycolytic intermediates in fibroblasts supplemented with 100% [1-^{13}C]-glucose at t = 0 hr.

(B) Glycolytic (f_{Glyc}) and oxidative PPP (f_{OxPPP}) flux ratio determined with the MID of PEP at 48 hr.

(C) Labeling fraction of m+0 to m+2 mass isotopomers for selected metabolites of fibroblasts treated without (ctrl) or with 500 μM H_2O_2 and cultured in media supplemented with 50% [U-^{12}C]-glucose and 50% of either [1-^{13}C]- or [2-^{13}C]-glucose.

(D) Ratio of fluxes entering directly from taken up glucose into oxidative PPP (f_{direct}) or after one or multiple cycle through oxidative PPP and entering back into oxidative PPP via upper glycolysis ($f_{cycling}$). The ratios were calculated using the m+0 fraction of 6PG in fibroblasts treated with or without 500 μM H_2O_2 for 10 min in media supplemented with [1-^{13}C]-glucose.

(E) Ratio of fluxes entering oxidative PPP in cells with or without transketo- and TA double knockdowns. Plots show mean values ± SD of three individual biological replicates in (A)–(C), (E), and of three independent experiments with three biological replicates each in (D). (Related to Figure S5; Table S6.)

The Acute Metabolic Response to Oxidative Stress Can Be Induced by Solar UV Irradiation and Is Necessary to Maintain Redox Homeostasis

UV irradiation is the most important natural inducer of oxidative stress in human skin. Therefore, we tested whether UV irradiation of skin cells would result in an acute metabolic response similar to H_2O_2 treatment. Fibroblasts and keratinocytes were irradiated for 0, 3, 6, and 9 min with solar simulated radiation (SSR/UV) (Fourtanier et al., 2005) and their metabolome analyzed by non-targeted metabolomics (Tables S3 and S4).

Already after 3 min exposure to UV, cells showed elevated levels of oxidative and non-oxidative PPP intermediates (Figure 5A and S6A–S6C). FBP levels initially dropped but were elevated after 6 and 9 min of irradiation. These metabolites patterns parallel those following H_2O_2 treatment (Figures 2 and S4C). To demonstrate that UV irradiation induces the same reorganization of PPP fluxes as H_2O_2 treatment, we performed ^{13}C-labeling experiments in skin fibroblasts and keratinocytes with medium containing 100% [1,2-^{13}C]-glucose (fibroblasts) or medium with 50% [U-^{12}C]-glucose and 50% [1,2-^{13}C]-glucose (keratinocytes) and exposed them to UV irradiation for up to 30 min. Comparably to H_2O_2, the m+1 fractions of upper glycolytic metabolites, including F6P and FBP, as well as of pentose phosphates increase upon treatment with UV, demonstrating increased backflux of carbons passing the oxidative branch of the PPP into upper glycolysis through the non-oxidative branch (Figures 5B and S5B; Table S6). To verify that UV-induced activation of the oxidative PPP is necessary for oxidative stress defense, we investigated the change in ROS levels and GSH/GSSG ratio in cells with perturbed PPP functionality. In fibroblasts with knockdowns of either G6PD or TK/TA, 6 min of SSR/UV resulted in higher ROS level and lower GSH:GSSG ratio (Figures 5C–5F). This corroborates that metabolic rerouting in the PPP induced by UV exposure is similar to the mechanism we described for H_2O_2, which is essential for acute ROS clearance.

We tested the relevance of the immediate stress-induced activation of the oxidative PPP by viability and DNA damage assays upon short oxidative stress in the range of a few minutes. Cell viability after 5 min treatment with 500 μM H_2O_2 was reduced in fibroblasts with G6PD knockdown, in which the acute response was previously shown to be largely suppressed (Figure S6E). Similarly, we found increased double-strand breaks after 10 min treatment with 250 μM H_2O_2 in fibroblasts with G6PD knockdown (Figure S6F). These results confirm that the immediate flux rerouting has an important physiological role in human skin cells upon acute oxidative stress.

Model for Immediate Activation of Oxidative PPP upon H_2O_2- or UV-Induced Oxidative Stress

Our rapid sampling data demonstrates that the sudden flux increase in oxidative PPP upon oxidative stress is independent from transcriptional control or inhibition of GAPDH. The question remained how this acute metabolic shift is induced. Recently it was demonstrated that G6PD activity could be regulated by pHsp27, TIGAR, or SIRT2 (Cosentino et al., 2011; Wang et al., 2014). We indeed found levels of pHsp27, but not TIGAR and other stress-related proteins such as p53 and P38, to be increased after 5 min of H_2O_2 treatment in human fibroblasts (Figures 6A and 6B). However, knockdown of Hsp27, TIGAR, or SIRT2 in fibroblasts did not suppress the short-term metabolic response of the PPP to H_2O_2 (Figure 6C). Notably, the statistically significant increase in hexose phosphate levels is marginal given the reduced response of control fibroblasts. Based on these results, none of Hsp27, TIGAR, and SIRT2 seem to drive acute activation of the oxidative PPP upon oxidative stress.

In absence of plausible protein-mediated activation, we thought of direct regulation of enzymes by small molecules because of the many allosteric interactions previously reported for glycolysis and PPP (Table S7). Two key metabolites that could directly activate flux into oxidative PPP are NADPH as G6PD inhibitor (Cho and Joshi, 1990; Holten et al., 1976; Ozer et al., 2001) and 6PG as PGI inhibitor (Kahana et al., 1960; Tsuboi et al., 1971). To specifically assess the transient NADPH levels, we analyzed metabolite extracts prepared without the drying step, which affects redox-sensitive species. As expected, levels of NADPH dropped and levels of 6PG increased significantly after 30 or 60 s H_2O_2 treatment in fibroblasts and keratinocytes (Figure S7A). Intracellular 6PG increased in fibroblasts more than 10-fold to >5 mM (Figure S7B). Since both 6PG and NADPH change immediately after stress induction, we tested their inhibitory potential on G6PD and PGI enzyme activity in crude protein extracts of keratinocytes and fibroblasts. We measured that NADPH but not NADH is a potent inhibitor of G6PD and reduces its activity by up to 80% (Figure 7A and S7D). In addition, 6PG was found to inhibit PGI by up to 90% (Figures 7B and S7C). These data lead to a mechanistic model of PPP activation where oxidative stress causes a drop in NADPH, which in turn reduces its inhibition of G6PD and increases the flux to 6PG. Accumulation of 6PG potentially amplifies the rerouting of carbon flux through G6PD by reducing PGI activity (Figure 7C).

DISCUSSION

Oxidative Stress Induces Immediate and Transient Metabolic Adaptations in Central Carbon and Nucleotide Metabolism

We investigated with extraordinary temporal detail and metabolism coverage the metabolic adaptations during H_2O_2- and UV-irradiation-induced oxidative stress in human skin cells using a non-targeted metabolomics approach. We found that within seconds, both stress conditions cause an acute and highly transient metabolic response. This entails primarily rerouting of metabolic flux in central carbon metabolism and purine biosynthesis and occurs before transcriptional changes ($\geq$40 min). In central carbon metabolism, we observed metabolic changes in TCA cycle, all of which are consistent with previously known oxidative inhibition of aconitase and α-ketoglutarate dehydrogenase (Chinopoulos et al., 1999; Nulton-Persson and Szweda, 2001; Tretter and Adam-Vizi, 2000). This blockage leads to a lower oxidative phosphorylation rate, causing a reduced generation of ATP, which was confirmed by the increase of the AMP:ATP ratio (Tavazzi et al., 2000), but even more importantly, it was suggested to reduce generation of endogenous ROS in the respiratory chain (Stowe and Camara, 2009; Tretter and Adam-Vizi, 2005).

The major response was observed at the interface of glycolysis and PPP. Our analysis demonstrated an immediate activation of the oxidative PPP coupled to a reduced glycolytic flux, indicated by an accumulation of PPP and upper glycolytic metabolites and a decrease of metabolites in lower glycolysis. The activation of oxidative PPP flux leads to an elevated reduction of $NADP^+$ to NADPH and thus increases the molecular currency needed to drive most ROS clearance mechanisms (Grant, 2008; Pollak et al., 2007; Ralser et al., 2007, 2009). Furthermore, increased flux into PPP provides building blocks for de novo biosynthesis of nucleotides, necessary for ROS-induced DNA

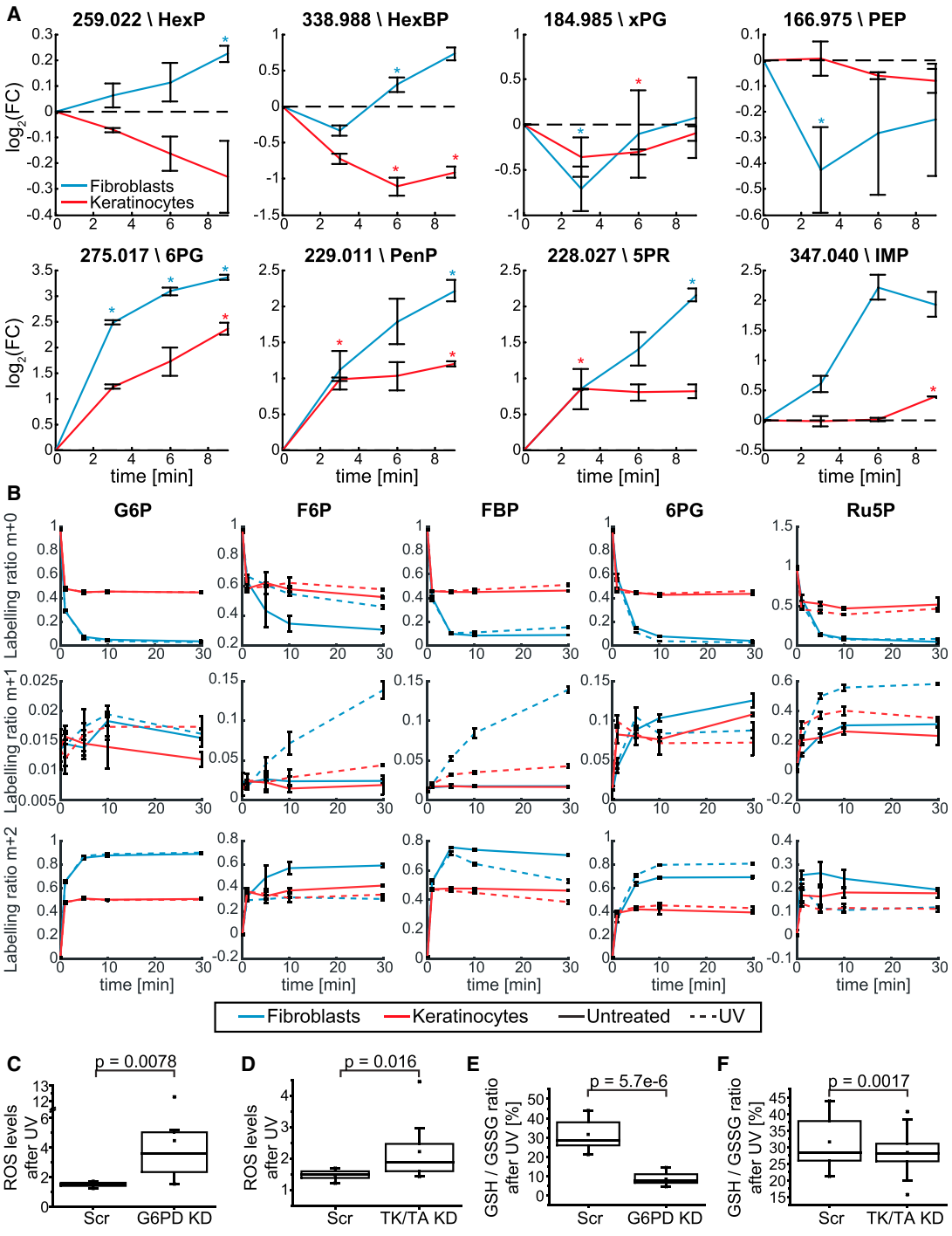

Figure 5. Metabolic and Phenotypic Response to UV Treatment in Fibroblasts and Keratinocytes

(A) Relative changes in metabolite levels in fibroblasts and keratinocytes after exposure to 0–9 min UV stress. Plots show mean values ± SEM, including results of a paired t test comparing metabolite levels at x versus 0 min UV treatment (*$p < 0.05$) of two (keratinocytes) and four (fibroblasts) individual experiments with three biological replicates each.

(B) Labeling fraction of m+0 – m+2 mass isotopomers for selected metabolites of fibroblasts and keratinocytes cultured in media supplemented with 100% [1,2-^{13}C]-glucose (fibroblasts) or 50% [U-^{12}C]-glucose and 50% of [1,2-^{13}C]-glucose (keratinocytes) that were exposed for up to 30 min UV stress. Plots show mean values ± SD of three individual biological replicates.

(C–F) ROS levels ([C] and [D]) and GSH/GSSG ration ([E] and [F]) in fibroblasts after 6 min of UV exposure targeted with control siRNA (SCR) and either ([C] and [E]) G6PD or ([D] and [F]) TK/TA siRNA. p values were determined for (C) and (D) with a Wilcoxon rank-sum test of eight individual experiments and for (E) and (F) with a paired t test of eight individual experiments (related to Figure S6; Tables S3 and S4).

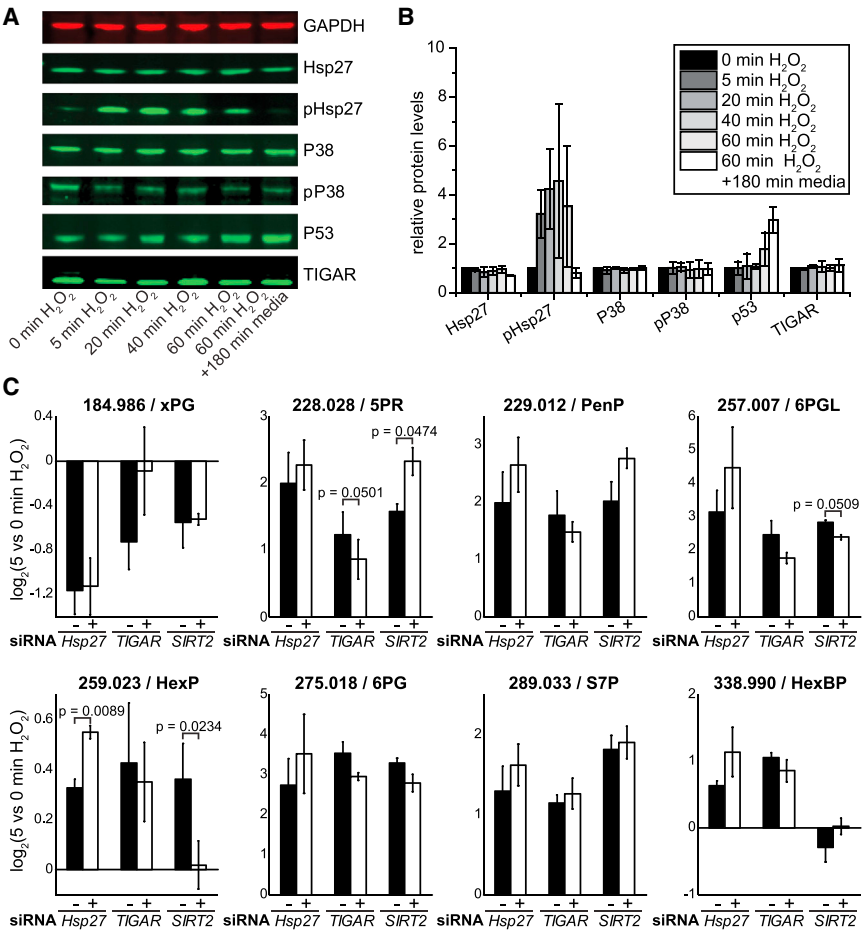

Figure 6. Influence of Hsp27, TIGAR, and SIRT2 on the Metabolic Adaptation in the PPP and Glycolysis upon Oxidative Stress

(A and B) (A) Western Blot and (B) quantification of relative changes in protein levels of GAPDH (control), Hsp27, pHsp27, P38, pP38, P53, and TIGAR after exposure to 500 μM H_2O_2. Bar plots in (B) show mean values ± SD of three individual experiments.

(C) Relative metabolite changes comparing untargeted metabolite measurements after and before exposure to 5 min of 500 μM H_2O_2 in fibroblasts transfected with control siRNA (–) or siRNA targeting (+) Hsp27, TIGAR, or SIRT2. Plots show the mean values ± SEM of the relative metabolite changes, including p values of paired t tests (all $p < 0.1$ are shown) of six (Hsp27) and three (TIGAR, SIRT2) individual experiments with each three biological replicates.

damage repair (Cooke et al., 2003; Marnett, 2000), which is supported by accumulation of 5PRA, the product of the commitment step into purine biosynthesis catalyzed by PPAT (Berg et al., 2002).

Model of Immediate PPP Activation upon Oxidative Stress

In yeast and other human cell types, it was shown that inhibition of glycolytic enzymes like GAPDH or PKM2 by oxidation leads to an accumulation of glycolytic intermediates that consequently induce an increased flux into PPP, both through the oxidative and non-oxidative branch (Anastasiou et al., 2011; Colussi et al., 2000; Ralser et al., 2007, 2009) (Figure S7E). Even though we observed an inhibited GAPDH activity upon oxidative stress, our data on sensitivity and timing of metabolic adaptations indicated that activation of the oxidative PPP is in fact largely independent of blockage of glycolytic flux through oxidation of GAPDH or PKM2. This hypothesis was verified in TK and TA knockdowns, which showed that intermediates in PPP accumulate primarily because of an increased flux through the oxidative PPP. Despite the highly transient state of the metabolic response, the ^{13}C-labeling patterns of 6PG demonstrated that under oxidative stress conditions the proportion of cycling flux into oxidative PPP increases 3-fold compared to non-stressed baseline flux. Carbon tracing experiments in TK/TA knockdown cells verified that carbon flux into oxidative PPP is partially originating through increased cycling flux in PPP. We therefore propose a model for the immediate response to acute oxidative stress in which oxidative PPP is immediately activated, leading to increased NADPH production and reversal of non-oxidative PPP compared to unstressed steady state (Figure 7C). This early redirection of flux is independent of the inhibition of glycolytic flux by GAPDH or PKM2, which, however, might favor carbon cycling in the PPP and thus maximize NADPH generation (Hanke et al., 2013; Kruger and von Schaewen, 2003; Siedler et al., 2012).

The rerouting of carbon into oxidative PPP depends on a rapid increase of the G6PD flux. Our data rules out that activation of G6PD is caused by transcriptional regulation, post-translation control by pHsp27 and TIGAR (Cosentino et al., 2011), or deacetylation by SIRT2 (Wang et al., 2014). By exclusion, we argue that oxidative flux rerouting is caused by either direct oxidation of G6PD, other unreported post-translational modifications, or allosteric interactions that affect its conformation and activity (Patra and Hay, 2014). A probable mechanism is direct inhibition by NADPH (Cho and Joshi, 1990; Holten et al., 1976; Ozer et al., 2001), which we could verify with own biochemical assays and is also consistent with the observed immediate drop in NADPH (Figures 1E and S7A). Such a regulatory mechanism brings about a purely demand-driven regeneration of NADPH during acute stress, which engages without temporal delays.

Overall, we show that the metabolic response of human skin cells to oxidative stress is highly dynamic and more complex than so far assumed. Even if transient in time and attenuated before onset of a response in gene expression, both the activation of oxidative PPP and inhibition of lower glycolysis are found to be important to counteract oxidative stress and to protect the

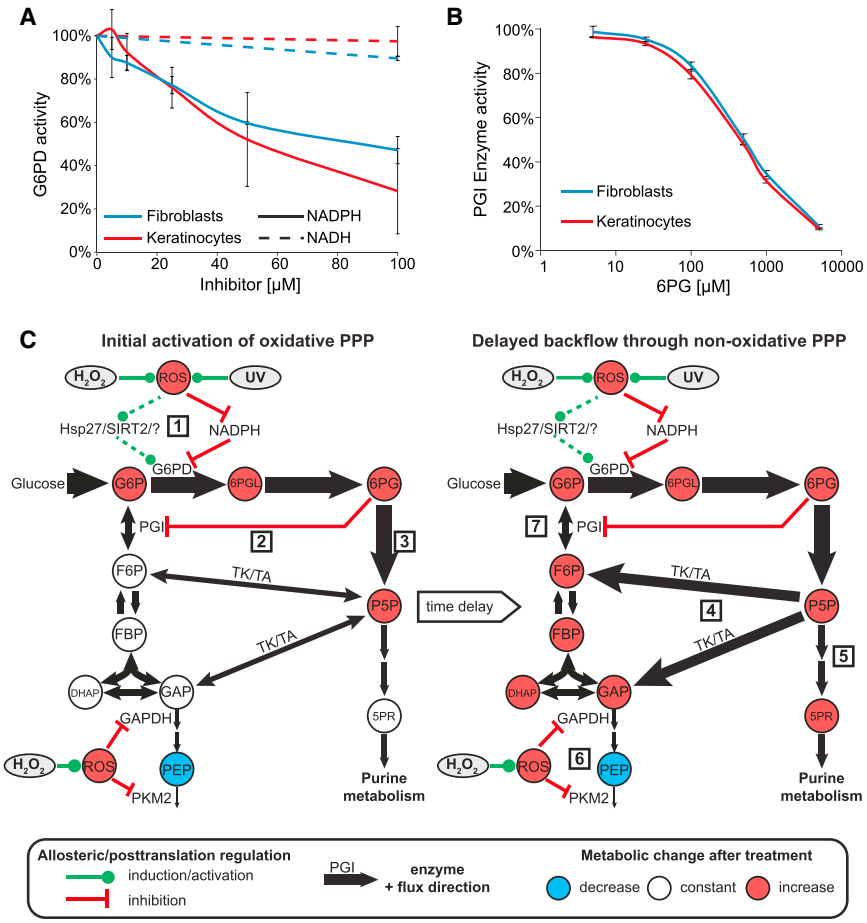

Figure 7. Model of the Acute Activation of the Oxidative PPP as Immediate Oxidative Stress Response in Human Skin Cells

(A and B) (A) Inhibitory effect of NADH and NADPH on G6PD enzyme activity with 25 μM $NADP^+$ as substrate and (B) inhibitory effect of 6PG on PGI enzyme activity in crude protein extracts of fibroblasts and keratinocytes. Plots show mean values ± SD of two individual experiments.

(C) Model for rerouting of metabolic flux in human skin cells during oxidative stress: (1) Initially, oxidative stress induces an immediate drop in NADPH, which potentially reduces its inhibition on G6PD and thereby activates the oxidative PPP. (2) Increased flux through the oxidative PPP leads to a strong accumulation of 6PG, a potent inhibitor of PGI, which could further increase flux into PPP by inhibiting PGI. (3) High flux through oxidative PPP consequently leads to an accumulation of pentose phosphates in the non-oxidative PPP, (4) forcing a delayed increased flux back into upper glycolysis and (5) nucleotide metabolism. (6) Due to the backflux and the reported inhibition of GAPDH by ROS, upper glycolytic metabolites accumulate, which can potentially lead to a reentry of carbon backbones into oxidative PPP via G6P, leading to a multiple cycling and a maximized NADPH production for oxidative stress defense (related to Figure S7; Table S7).

cells from impaired redox homeostasis and oxidative-stress-induced damage. This immediate response may have an important role in other tissues as first-line defense to instantaneously fight oxidative stress before the onset of transcriptional responses. For instance, late-stage cancers counterbalance excessive ROS generation by expression of different antioxidant systems mainly via the transcription factor Nrf2, which is positively regulated by ROS and also activates NAPDH-producing enzymes such as G6PD and 6PGDH (Mitsuishi et al., 2012; Polimeni et al., 2011). Exogenously increasing intracellular ROS is a common therapy to selectively induce cell death in cancer cells whose anti-oxidant capacity is saturated by endogenous and exogenous ROS (Gorrini et al., 2013; Trachootham et al., 2009). Direct activation of PPP upon oxidative stress may protect cancer cells from cellular damage induced by ROS-based therapeutics within the first minutes of therapy until expression of antioxidant systems continuously protect against the stress.

EXPERIMENTAL PROCEDURES

Induction of Oxidative Stress in Human Skin Cells

For all oxidative stress experiments, 3 × 10^5 human neonatal fibroblasts (Tebu-Bio) or 1 × 10^5 neonatal human epidermal keratinocytes (Lonza) were seeded and cultivated for 72 hr at 37°C and 5% CO_2. For induction of oxidative stress with H_2O_2 (Sigma-Aldrich), culture medium was replaced with H_2O_2-supplemented medium and cells incubated for the indicated time. For UV-induced oxidative stress, cells were irradiated with SSR of an Oriel UV sun simulator (LOT) in phenol-red-free culture medium. For gene knockdown, primary fibroblasts were transfected with siRNA (QIAGEN) utilizing the Neon transfection system (Invitrogen) according to manufacturer's instructions. Further details can be found in the Supplemental Information.

Metabolite Measurements

For the analysis of the intracellular metabolome of human skin cells, cells were washed with 75 mM ammonium carbonate at pH 7.4 and quenched using liquid nitrogen. Intracellular metabolites were extracted twice with 70% ethanol at 75°C for 3 min, dried in a speedvac, and resuspended in H_2O for mass spectrometric analysis. Non-targeted metabolite profiling was performed by flow injection analysis on an Agilent 6550 QTOF (Agilent) in negative mode as reported earlier (Fuhrer et al., 2011). Ions were annotated to metabolites based on exact mass using the HMDB v3.0 database (Wishart et al., 2013). Quantitative targeted analysis and analysis of MIDs were performed using ultra-high-pressure chromatography-coupled tandem mass spectrometry as described before (Buescher et al., 2010; Rühl et al., 2012). Mass isotopomers were corrected for natural abundance of ^{13}C as previously described (Yuan et al., 2008). Details can be found in the Supplemental Experimental Procedures.

Intracellular Glutathione and ROS Assays

To determine the change of intracellular GSH/GSSG ratio and ROS levels after exposure to oxidative stress, 10^4 fibroblasts/well were seeded in a 96-well plate and cultivated for 24 hr. Oxidative stress was induced by irradiation with SSR in phenol-red-free DMEM for 6 min. Control cells were treated with phenol-red-free DMEM for 6 min. The ratio of reduced to oxidized glutathione (GSH/GSSG) was measured using the GSH/GSSG Glo Assay Kit (Promega) according to the manufacturer's instructions. ROS levels were quantified at an excitation/emission of 495 nm/520 nm using 2′,7′-dichlorofluorescein

(DCF) with which the cells were incubated for 30 min at 37°C at a concentration of 150 μg/ml in PBS.

G6PD and PGI Enzyme Assay

G6PD enzyme assay in crude protein extracts was performed in potassium phosphate buffer at pH 7 supplemented with 5 mM $MgCl_2$ at 37°C, with G6P and $NAPD^+$ as substrate and NADPH or NADH as inhibitor. PGI enzymes assays were performed using Phosphoglucose Isomerase Colorimetric Assay Kit (Sigma-Aldrich) with 1/10 of the substrate and 6PG as inhibitor. Enzyme activities were determined by monitoring the product formation in a plate reader. Details can be found in the Supplemental Experimental Procedures.

SUPPLEMENTAL INFORMATION

Supplemental Information includes seven figures, seven tables, and Supplemental Experimental Procedures and can be found with this article online at http://dx.doi.org/10.1016/j.molcel.2015.06.017.

AUTHOR CONTRIBUTIONS

H.E. performed most of the experiments. A.K. did part of the experiments and all the mass spectrometric measurements, including computational data analysis. H.E. and A.K. designed the experiments together, wrote the manuscript together, and contributed equally to this work. J.S. performed the labeling experiments under UV conditions. J.H. and N.Z. advised on experimental design, data interpretation, and writing of the manuscript. M.W. and F.F. supervised the analyses. H.W., R.L., S.G., and L.T. assisted with interpretation of the results.

ACKNOWLEDGMENTS

We thank Tobias Fuhrer and Manuel Hörl for their support in interpreting the ^{13}C-labelling experiments. This work was partially funded by SystemsX.ch (IPhD grant to A.K.).

H.E., J.S., M.W., F.F., H.W., S.G., L.T., and J.H. are employees of Beiersdorf AG. This work was supported in part by a grant from Beiersdorf AG.

Received: December 20, 2014
Revised: May 12, 2015
Accepted: June 10, 2015
Published: July 16, 2015

REFERENCES

Anastasiou, D., Poulogiannis, G., Asara, J.M., Boxer, M.B., Jiang, J.K., Shen, M., Bellinger, G., Sasaki, A.T., Locasale, J.W., Auld, D.S., et al. (2011). Inhibition of pyruvate kinase M2 by reactive oxygen species contributes to cellular antioxidant responses. Science *334*, 1278–1283.

Berg, J.M., Tymoczko, J.L., and Stryer, L. (2002). Section 25.2. In Biochemistry (W.H. Freeman).

Buescher, J.M., Moco, S., Sauer, U., and Zamboni, N. (2010). Ultrahigh performance liquid chromatography-tandem mass spectrometry method for fast and robust quantification of anionic and aromatic metabolites. Anal. Chem. *82*, 4403–4412.

Chen, L., Hu, J.Y., and Wang, S.Q. (2012). The role of antioxidants in photoprotection: a critical review. J. Am. Acad. Dermatol. *67*, 1013–1024.

Chinopoulos, C., Tretter, L., and Adam-Vizi, V. (1999). Depolarization of in situ mitochondria due to hydrogen peroxide-induced oxidative stress in nerve terminals: inhibition of alpha-ketoglutarate dehydrogenase. J. Neurochem. *73*, 220–228.

Cho, S.W., and Joshi, J.G. (1990). Characterization of glucose-6-phosphate dehydrogenase isozymes from human and pig brain. Neuroscience *38*, 819–828.

Colussi, C., Albertini, M.C., Coppola, S., Rovidati, S., Galli, F., and Ghibelli, L. (2000). H2O2-induced block of glycolysis as an active ADP-ribosylation reaction protecting cells from apoptosis. FASEB J. *14*, 2266–2276.

Cooke, M.S., Evans, M.D., Dizdaroglu, M., and Lunec, J. (2003). Oxidative DNA damage: mechanisms, mutation, and disease. FASEB J. *17*, 1195–1214.

Cosentino, C., Grieco, D., and Costanzo, V. (2011). ATM activates the pentose phosphate pathway promoting anti-oxidant defence and DNA repair. EMBO J. *30*, 546–555.

Fan, J., Ye, J., Kamphorst, J.J., Shlomi, T., Thompson, C.B., and Rabinowitz, J.D. (2014). Quantitative flux analysis reveals folate-dependent NADPH production. Nature *510*, 298–302.

Fang, Y.Z., Yang, S., and Wu, G. (2002). Free radicals, antioxidants, and nutrition. Nutrition *18*, 872–879.

Finkel, T. (2003). Oxidant signals and oxidative stress. Curr. Opin. Cell Biol. *15*, 247–254.

Finkel, T., and Holbrook, N.J. (2000). Oxidants, oxidative stress and the biology of ageing. Nature *408*, 239–247.

Fourtanier, A., Moyal, D., Maccario, J., Compan, D., Wolf, P., Quehenberger, F., Cooper, K., Baron, E., Halliday, G., Poon, T., et al. (2005). Measurement of sunscreen immune protection factors in humans: a consensus paper. J. Invest. Dermatol. *125*, 403–409.

Fuhrer, T., Heer, D., Begemann, B., and Zamboni, N. (2011). High-throughput, accurate mass metabolome profiling of cellular extracts by flow injection-time-of-flight mass spectrometry. Anal. Chem. *83*, 7074–7080.

Gorrini, C., Harris, I.S., and Mak, T.W. (2013). Modulation of oxidative stress as an anticancer strategy. Nat. Rev. Drug Discov. *12*, 931–947.

Grant, C.M. (2008). Metabolic reconfiguration is a regulated response to oxidative stress. J. Biol. *7*, 1.

Hanke, T., Noh, K., Noack, S., Polen, T., Bringer, S., Sahm, H., Wiechert, W., and Bott, M. (2013). Combined fluxomics and transcriptomics analysis of glucose catabolism via a partially cyclic pentose phosphate pathway in Gluconobacter oxydans 621H. Appl. Environ. Microbiol. *79*, 2336–2348.

Hillar, A., and Nicholls, P. (1992). A mechanism for NADPH inhibition of catalase compound II formation. FEBS Lett. *314*, 179–182.

Holten, D., Procsal, D., and Chang, H.L. (1976). Regulation of pentose phosphate pathway dehydrogenases by NADP+/NADPH ratios. Biochem. Biophys. Res. Commun. *68*, 436–441.

Kahana, S.E., Lowry, O.H., Schulz, D.W., Passonneau, J.V., and Crawford, E.J. (1960). The kinetics of phosphoglucoisomerase. J. Biol. Chem. *235*, 2178–2184.

Kanavy, H.E., and Gerstenblith, M.R. (2011). Ultraviolet radiation and melanoma. Semin. Cutan. Med. Surg. *30*, 222–228.

Kirkman, H.N., Galiano, S., and Gaetani, G.F. (1987). The function of catalase-bound NADPH. J. Biol. Chem. *262*, 660–666.

Kohen, R., and Nyska, A. (2002). Oxidation of biological systems: oxidative stress phenomena, antioxidants, redox reactions, and methods for their quantification. Toxicol. Pathol. *30*, 620–650.

Kruger, N.J., and von Schaewen, A. (2003). The oxidative pentose phosphate pathway: structure and organisation. Curr. Opin. Plant Biol. *6*, 236–246.

Liebermann, D.A., and Hoffman, B. (2008). Gadd45 in stress signaling. J. Mol. Signal. *3*, 15.

Marnett, L.J. (2000). Oxyradicals and DNA damage. Carcinogenesis *21*, 361–370.

Martindale, J.L., and Holbrook, N.J. (2002). Cellular response to oxidative stress: signaling for suicide and survival. J. Cell. Physiol. *192*, 1–15.

Mitsuishi, Y., Taguchi, K., Kawatani, Y., Shibata, T., Nukiwa, T., Aburatani, H., Yamamoto, M., and Motohashi, H. (2012). Nrf2 redirects glucose and glutamine into anabolic pathways in metabolic reprogramming. Cancer Cell *22*, 66–79.

Nulton-Persson, A.C., and Szweda, L.I. (2001). Modulation of mitochondrial function by hydrogen peroxide. J. Biol. Chem. *276*, 23357–23361.

Ozer, N., Aksoy, Y., and Ogüs, I.H. (2001). Kinetic properties of human placental glucose-6-phosphate dehydrogenase. Int. J. Biochem. Cell Biol. *33*, 221–226.

Pai, E.F., and Schulz, G.E. (1983). The catalytic mechanism of glutathione reductase as derived from x-ray diffraction analyses of reaction intermediates. J. Biol. Chem. *258*, 1752–1757.

Patra, K.C., and Hay, N. (2014). The pentose phosphate pathway and cancer. Trends Biochem. Sci. *39*, 347–354.

Polimeni, M., Voena, C., Kopecka, J., Riganti, C., Pescarmona, G., Bosia, A., and Ghigo, D. (2011). Modulation of doxorubicin resistance by the glucose-6-phosphate dehydrogenase activity. Biochem. J. *439*, 141–149.

Pollak, N., Dölle, C., and Ziegler, M. (2007). The power to reduce: pyridine nucleotides—small molecules with a multitude of functions. Biochem. J. *402*, 205–218.

Qiu, X., Forman, H.J., Schönthal, A.H., and Cadenas, E. (1996). Induction of p21 mediated by reactive oxygen species formed during the metabolism of aziridinylbenzoquinones by HCT116 cells. J. Biol. Chem. *271*, 31915–31921.

Ralser, M., Wamelink, M.M., Kowald, A., Gerisch, B., Heeren, G., Struys, E.A., Klipp, E., Jakobs, C., Breitenbach, M., Lehrach, H., and Krobitsch, S. (2007). Dynamic rerouting of the carbohydrate flux is key to counteracting oxidative stress. J. Biol. *6*, 10.

Ralser, M., Wamelink, M.M., Latkolik, S., Jansen, E.E., Lehrach, H., and Jakobs, C. (2009). Metabolic reconfiguration precedes transcriptional regulation in the antioxidant response. Nat. Biotechnol. *27*, 604–605.

Ray, P.D., Huang, B.W., and Tsuji, Y. (2012). Reactive oxygen species (ROS) homeostasis and redox regulation in cellular signaling. Cell. Signal. *24*, 981–990.

Rescigno, M., and Perham, R.N. (1994). Structure of the NADPH-binding motif of glutathione reductase: efficiency determined by evolution. Biochemistry *33*, 5721–5727.

Rühl, M., Rupp, B., Nöh, K., Wiechert, W., Sauer, U., and Zamboni, N. (2012). Collisional fragmentation of central carbon metabolites in LC-MS/MS increases precision of ^{13}C metabolic flux analysis. Biotechnol. Bioeng. *109*, 763–771.

Shenton, D., and Grant, C.M. (2003). Protein S-thiolation targets glycolysis and protein synthesis in response to oxidative stress in the yeast Saccharomyces cerevisiae. Biochem. J. *374*, 513–519.

Siedler, S., Bringer, S., Blank, L.M., and Bott, M. (2012). Engineering yield and rate of reductive biotransformation in Escherichia coli by partial cyclization of the pentose phosphate pathway and PTS-independent glucose transport. Appl. Microbiol. Biotechnol. *93*, 1459–1467.

Stincone, A., Prigione, A., Cramer, T., Wamelink, M.M., Campbell, K., Cheung, E., Olin-Sandoval, V., Grüning, N., Krüger, A., Tauqeer Alam, M., et al. (2014). The return of metabolism: biochemistry and physiology of the pentose phosphate pathway. Biol. Rev. Camb. Philos. Soc. http://dx.doi.org/10.1111/brv.12140.

Stowe, D.F., and Camara, A.K. (2009). Mitochondrial reactive oxygen species production in excitable cells: modulators of mitochondrial and cell function. Antioxid. Redox Signal. *11*, 1373–1414.

Tavazzi, B., Di Pierro, D., Amorini, A.M., Fazzina, G., Tuttobene, M., Giardina, B., and Lazzarino, G. (2000). Energy metabolism and lipid peroxidation of human erythrocytes as a function of increased oxidative stress. Eur. J. Biochem. *267*, 684–689.

Tiwari, B.S., Belenghi, B., and Levine, A. (2002). Oxidative stress increased respiration and generation of reactive oxygen species, resulting in ATP depletion, opening of mitochondrial permeability transition, and programmed cell death. Plant Physiol. *128*, 1271–1281.

Trachootham, D., Alexandre, J., and Huang, P. (2009). Targeting cancer cells by ROS-mediated mechanisms: a radical therapeutic approach? Nat. Rev. Drug Discov. *8*, 579–591.

Tretter, L., and Adam-Vizi, V. (2000). Inhibition of Krebs cycle enzymes by hydrogen peroxide: A key role of [alpha]-ketoglutarate dehydrogenase in limiting NADH production under oxidative stress. J. Neurosci. *20*, 8972–8979.

Tretter, L., and Adam-Vizi, V. (2005). Alpha-ketoglutarate dehydrogenase: a target and generator of oxidative stress. Philos. Trans. R. Soc. Lond. B Biol. Sci. *360*, 2335–2345.

Tsuboi, K.K., Fukunaga, K., and Chervenka, C.H. (1971). Phosphoglucose isomerase from human erythrocyte. Preparation and properties. J. Biol. Chem. *246*, 7586–7594.

Wang, Y.P., Zhou, L.S., Zhao, Y.Z., Wang, S.W., Chen, L.L., Liu, L.X., Ling, Z.Q., Hu, F.J., Sun, Y.P., Zhang, J.Y., et al. (2014). Regulation of G6PD acetylation by SIRT2 and KAT9 modulates NADPH homeostasis and cell survival during oxidative stress. EMBO J. *33*, 1304–1320.

Wishart, D.S., Jewison, T., Guo, A.C., Wilson, M., Knox, C., Liu, Y., Djoumbou, Y., Mandal, R., Aziat, F., Dong, E., et al. (2013). HMDB 3.0—The Human Metabolome Database in 2013. Nucleic Acids Res. *41* (Database issue), D801–D807.

Xiong, Y., Hannon, G.J., Zhang, H., Casso, D., Kobayashi, R., and Beach, D. (1993). p21 is a universal inhibitor of cyclin kinases. Nature *366*, 701–704.

Ying, W. (2008). NAD+/NADH and NADP+/NADPH in cellular functions and cell death: regulation and biological consequences. Antioxid. Redox Signal. *10*, 179–206.

Yuan, J., Bennett, B.D., and Rabinowitz, J.D. (2008). Kinetic flux profiling for quantitation of cellular metabolic fluxes. Nat. Protoc. *3*, 1328–1340.